

Observation of tunable single-atom Yu-Shiba-Rusinov statesArtem Odobesko^{1,*}, Domenico Di Sante^{2,†}, Alexander Kowalski², Stefan Wilfert¹, Felix Friedrich¹, Ronny Thomale², Giorgio Sangiovanni² and Matthias Bode^{1,3}¹*Physikalisches Institut, Experimentelle Physik II, Universität Würzburg, Am Hubland, 97074 Würzburg, Germany*²*Institut für Theoretische Physik und Astrophysik and Würzburg-Dresden Cluster of Excellence ct.qmat, Universität Würzburg, Am Hubland Campus Süd, Würzburg 97074, Germany*³*Wilhelm Conrad Röntgen-Center for Complex Material Systems (RCCM), Universität Würzburg, Am Hubland, 97074 Würzburg, Germany* (Received 18 April 2020; revised 26 October 2020; accepted 27 October 2020; published 13 November 2020)

The coupling of a spin to an underlying substrate is the basis for a plethora of phenomena. In the case of a metallic substrate, Kondo screening of the adatom magnetic moment can occur. As the substrate turns superconducting, an intriguing situation emerges where pair breaking due to the adatom spins leads to Yu-Shiba-Rusinov bound states, but also intertwines with Kondo phenomena. Through scanning tunneling spectroscopy, we analyze the interdependence of Kondo screening and superconductivity. Our data obtained on single Fe adatoms on Nb(110) show that the coupling and the resulting YSR states are strongly adsorption site-dependent and reveal a quantum phase transition at a Kondo temperature comparable to the superconducting gap. The experimental signatures are rationalized by combined density-functional theory and continuous-time quantum Monte Carlo calculations to rigorously treat magnetic and hybridization effects on equal footing.

DOI: [10.1103/PhysRevB.102.174504](https://doi.org/10.1103/PhysRevB.102.174504)**I. INTRODUCTION**

Chains of magnetic atoms on the surface of a highly spin-orbit-coupled superconductor were the basis for the discovery of Majorana zero modes (MZMs), which have been predicted [1–6] and reported [7–9] to exist at the ends of one-dimensional spin systems. Constant efforts have been undertaken for improving the properties of such hybrid systems. One crucial aspect is to precisely control the chain structure and length, which has been achieved by atomic manipulation on refractory substrates [8]. Another important parameter is how the magnetic adatoms couple to the substrate.

Spin-dependent scattering off a magnetic impurity on a superconductor gives rise to Yu-Shiba-Rusinov (YSR) states [10–12]. If assembled to atomic chains, the interacting impurities form YSR bands. To enter a topologically nontrivial phase on an *s*-wave superconductor, the YSR bands have to cross the Fermi level E_F . In a classical picture, the energy position of the YSR resonances with respect to E_F is a function of the local impurity spin and of the coupling to the substrate's conduction electrons. The description of a quantum impurity on a metallic substrate is instead a challenging task, which requires a full many-body treatment of the impurity and of the superconductor on equal footing. In the normal-metallic phase ($T > T_c$) the screening can lead to a drastic reduction or even the complete quenching of the impurity spin by a Kondo singlet cloud [13]. Below T_c , the Kondo effect intertwines with localized YSR states.

In the simplified picture of an $S = 1/2$ impurity on a superconductor, two limiting situations occur: In the strong-coupling regime, i.e., $k_B T_K \gg \Delta$, with the Boltzmann constant k_B , the Kondo temperature T_K , and the superconducting gap Δ , magnetic scattering results in pair breaking and leads to a Kondo resonance with a characteristic energy scale $k_B T_K$ [14]. Conversely, at very weak coupling ($k_B T_K \ll \Delta$) the pair-breaking effect almost vanishes and YSR resonances appear close to the edge of the superconducting gap. The intermediate situation ($k_B T_K \approx \Delta$) is determined by an involved interplay between the two effects. Theory predicts a quantum phase transition (QPT) between the two limiting cases at $k_B T_K \approx 0.3\Delta$, where the two YSR resonances cross E_F [15–17].

The coupling between magnetic impurities and the superconducting host has recently been investigated in several material systems: for MnPc molecules on Pb(111) [18,19], subtle changes of the molecule adsorption site caused a significant change in the YSR states energy with a QPT at $k_B T_K \approx \Delta$; in multi-impurity Kondo systems such as artificially created Fe clusters on Ta(100) [9]; for various 3d transition-metal atoms on superconducting Re(0001) surface [20]; and artificially induced coupling with a STM tip of MnPc molecules on a NbSe₂ substrate [21]. Also the role of impurity-substrate hybridization was investigated within the Anderson impurity model on oxygen vacancies on V(110) [22]. Thus the systematic understanding of screening effects of magnetic moments hybridizing with normal-metallic and superconducting surfaces represents an important cornerstone of engineered topological devices.

Here we present scanning tunneling spectroscopy (STS) data for single Fe adatoms adsorbed on various Nb(110)-derived surfaces. The individual Fe atoms are weakly coupled

*artem.odobesko@physik.uni-wuerzburg.de

†domenico.disante@physik.uni-wuerzburg.de

to the clean Nb(110) substrate, as indicated by YSR states, which strongly overlap with the superconducting gap edges. Our results indicate, however, that the coupling can be strongly enhanced by the vicinity of oxygen.

The YSR states of Fe atoms adsorbed close to or on top of oxygen-reconstructed areas (NbO_x) shift toward and eventually cross the Fermi level E_F at $k_B T_K \approx 0.7\Delta$, indicative of a QPT. By a magnetic-field-induced quenching of the superconducting state we prove that this QPT is accompanied by an increased Kondo temperature. Combined first-principles density-functional theory (DFT) and continuous-time quantum Monte Carlo (CT-QMC) calculations show that a subtle reduction of the Fe–Nb binding distance in the presence of oxygen results in an enhanced hybridization of the impurity atomic orbitals with the substrate, even sizable enough to overcompensate the oxygen-induced reduction of the Fe magnetic moment by a factor of two.

II. EXPERIMENTAL AND THEORETICAL METHODS

A clean Nb(110) surface with less than 10% NbO_x was prepared by heating up to $T = 2410^\circ\text{C}$ [23]. Scanning tunneling microscopy (STM) measurements were performed at $T_{\text{min}} = 1.17$ K. Fe atoms were evaporated *in situ* onto a cold Nb surface at $T = 4.2$ K. For increased energy resolution, the W tips were gently poked into the Nb sample to create a superconducting tip apex, resulting in a shift of all spectral features by $\pm\Delta_{\text{tip}}/e$. The tip's superconducting gap was determined to be $\Delta_{\text{tip}} = 1.28$ meV, slightly below the known gap size of Nb(110), $\Delta_{\text{Nb}} = 1.53$ meV [23]. For the better evaluation of relative YSR spectral intensities we numerically deconvoluted the tunneling spectra to remove the effect of the superconducting tip [24]. DFT calculations were performed by using the VASP simulation package [25], while the solution of the Anderson impurity model (AIM) was achieved by the hybridization-expansion CT-QMC method within the w2DYNAMICS code [26]. We have used a uniform Kanamori interaction parametrized by $U = 3.85$ eV and $J^{\text{Hund}} = 0.72$ eV [27]. More details are given in Ref. [24].

III. RESULTS

One major obstacle toward a systematic investigation of a direct correlation between the Kondo effect and YSR states is the difficulty in tuning the adatom–substrate coupling. As will be shown, a single magnetic Fe atom adsorbed on top of a clean Nb(110) surface offers a wide range of substrate-tunability scenarios, which allows systematic investigation of a direct correlation between the Kondo screening effect and YSR states. Figure 1(a) shows an atomic resolution STM image of a typical Nb(110) surface [23] after low-temperature deposition of Fe. Since the surface is not perfectly clean but contains a few oxygen-reconstructed patches (dark stripes), Fe adatoms in different adsorption sites can be found. Four examples are indicated by colored circles. As we show below, Fe exhibits a striking adsorption site-dependent coupling to the superconducting substrate, which allows us to systematically investigate the characteristic behavior expected for magnetic adatom–substrate coupling. The atoms marked as ① and ② are adsorbed on clean Nb(110). Unfortunately, the large

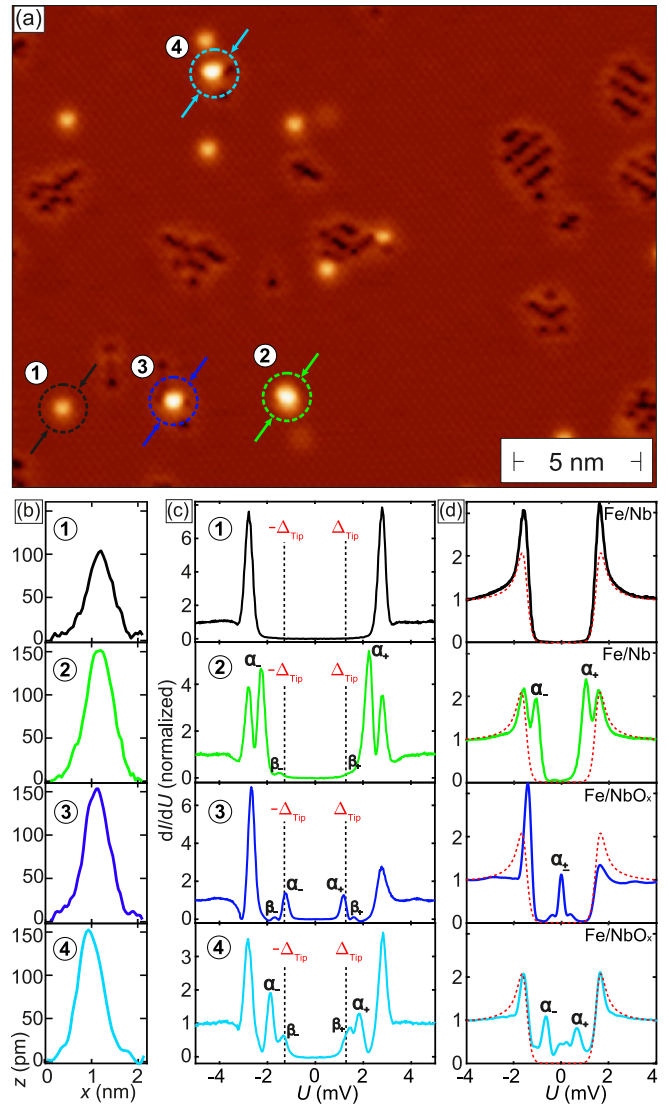


FIG. 1. (a) STM image of Fe adatoms on Nb(110). Stabilization parameters: $U = -0.6$ V, $I = 0.4$ nA, $T = 1.17$ K. (b) Line profiles measured between the arrows in panel (a) for the two Fe/Nb(110) in a H_4 site (black ①) and in a bridge site (green ②), respectively, and for two Fe atoms atop NbO_x (blue ③ and cyan ④). (c) Raw tunneling spectra as measured on the Fe atoms ①–④ with a superconducting tip and (d) their respective numerically deconvoluted spectra. The spectrum shown as a hatched red line is taken on the pristine Nb(110) surface. Stabilization parameters: $U = -7$ mV, $I = 0.4$ nA.

apparent diameter of the Fe adatom (≈ 1 nm) inhibits a precise experimental determination of the adsorption site inside the Nb(110) unit cell. Based on our DFT total-energy calculations we assume that these atoms are adsorbed in a fourfold hollow site (H_4) and in a threefold hollow site (H_{4d}), respectively [24]. As can be seen by the atom's brightness, their respective corrugation heights are significantly different. Line sections drawn across these atoms are displayed in Fig. 1(b). Atom ① has a height of ≈ 100 pm, while atom ② has a height of ≈ 150 pm and therefore appears brighter. The other two Fe atoms marked as ③ and ④ are located very close to or on top

of small oxygen-reconstructed patches and are both imaged as “bright” atoms with a height of ≈ 150 pm.

These different adsorption sites substantially impact the interaction with the substrate, as revealed by tunneling spectra measured above the respective Fe atoms [Fig. 1(c) shows raw data and Fig. 1(d) shows deconvoluted data]. The spectrum measured on ① qualitatively resembles the spectrum of pristine Nb (red hatched line) but exhibits enhanced coherence peaks. This observation corresponds to the weak-coupling limit described above, suggesting an extremely small exchange coupling with the superconductor. In contrast, all other types of Fe adatoms exhibit additional in-gap peaks. For example, the rare case with atom ② on clean Nb(110) shows fingerprints of YSR resonances close to the gap edge with strongly pronounced α_{\pm} and much weaker β_{\pm} peaks; see green spectra in Fig. 1(c). The electron-hole ($e^{-}h^{+}$) asymmetry of the spectral density of the YSR resonances originates from the local crystal field acting on the adatom from the Coulomb multiplet of the Fe d shell [18,28–30].

Fe atoms adsorbed close to or within the NbO_x unit cell exhibit tunneling spectra with α_{\pm} peaks further inside the superconducting gap, as exemplarily shown for ③ and ④. In contrast, the in-gap position of the weaker β_{\pm} peaks remains almost unchanged. For Fe atom ③ the deconvoluted data in Fig. 1(d) (blue curve) reveal that the α_{\pm} peaks coincide at E_F , a situation hardly distinguishable from a MZM. It is important to note, that—in comparison to Fe atom ②—the spectral density of the α_{\pm} peaks of Fe atom ④ appears with an inverted $e^{-}h^{+}$ asymmetry, indicating a transition toward the strong-coupling regime.

To verify that it is exactly the presence of oxygen which causes the observed changes we present what we consider a smoking-gun experiment in Fig. 2. In these experiments we use the STM tip to move individual Fe atoms out of or into the NbO_x area and examine the evolution of YSR states after each movement step. The STM images of the initial state and after each manipulation step are marked with numbers in Fig. 2(a). The corresponding tunneling spectra on the pertinent Fe atoms are shown in Fig. 2(b). All spectra are normalized, were measured in the same voltage range, and are shifted vertically for better visibility. In the initial configuration, which is shown in the top panel of Fig. 2(a), the Fe atom marked ① appears much brighter than the surrounding Fe adatoms. A tunneling spectrum recorded with the STM tip positioned on top of ① reveals several in-gap YSR states, see Fig. 2(b). As this Fe atom is moved away from its initial position, it turns darker, indicating a significant decrease of its apparent height. Furthermore, it becomes obvious that the surface underneath the initial adsorption site consists of NbO_x (dark area). In agreement with the results presented in Fig. 1 the spectrum of the Fe atom after manipulation [black dashed line ② in Fig. 2(b)], which is now known to be adsorbed on clean Nb(110), shows no YSR states. Similarly, the spectrum taken over the oxygen patch [cyan line O_x in Fig. 2(b)] does not show any feature inside the gap. Afterwards, Fe atom ③, which showed a featureless tunneling spectrum before manipulation, was moved close to the oxygen patch, resulting in a brighter appearance in constant-current STM images and clearly visible YSR peaks inside the gap [green curve ④ in Fig. 2(b)]. In ⑤ and ⑥ the same Fe atom is slightly shifted towards the center of oxygen

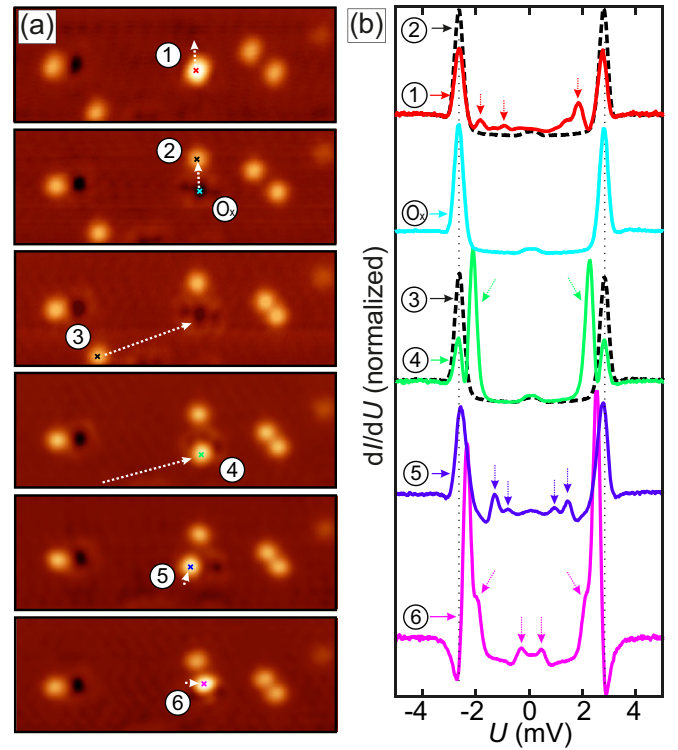


FIG. 2. Fe atom manipulation experiment in vicinity of NbO_x performed at $T = 4.2$ K. (a) STM images of the initial Fe adatom distribution (top) and after each movement step. White arrows represent the path along which the Fe atom has been moved. (b) Tunneling spectra taken on the Fe atoms at the position marked by circled numbers. Note that the spectra are vertically shifted for better visibility. Stabilization parameters: $U = -10$ mV, $I = 0.4$ nA.

patch, resulting in YSR resonances which progressively shift towards E_F .

In the vanishing- T_K limit, in which the impurity local moment can be described as a classical spin, the position of YSR states inside the superconducting gap is given by $|\varepsilon| = \Delta[(1 - a^2)/(1 + a^2)]$, where $a = Jm\pi\rho_s$ depends on the exchange interaction J , the impurity magnetic moment m , and the normal metallic density of states (DOS) ρ_s at E_F [15–17,19]. The presence of oxygen adsorbates affects the magnetic moment of the impurities [31] and in many cases causes its significant reduction [32,33]. Along this line of reasoning the observation of a stronger coupling on NbO_x is at first surprising. To shed light on this unexpected experimental finding we performed combined DFT and CT-QMC calculations, which allow us to go beyond the classical description and thereby also access the strong-coupling regime. As we show below, this gives full account of the many-body properties of the interacting impurity on the Nb substrate, remarkably without explicitly considering its superconducting phase.

The first step is to investigate single Fe atoms in their characteristic adsorption sites by DFT. The respective unit cells are presented in Fig. 3(a). We find equilibrium distances of 170 pm for Fe/Nb(110) and 134 pm for Fe/ NbO_x . As confirmed by the calculated charge-density profiles presented in Fig. 3(b), this leads to a higher charge density for the

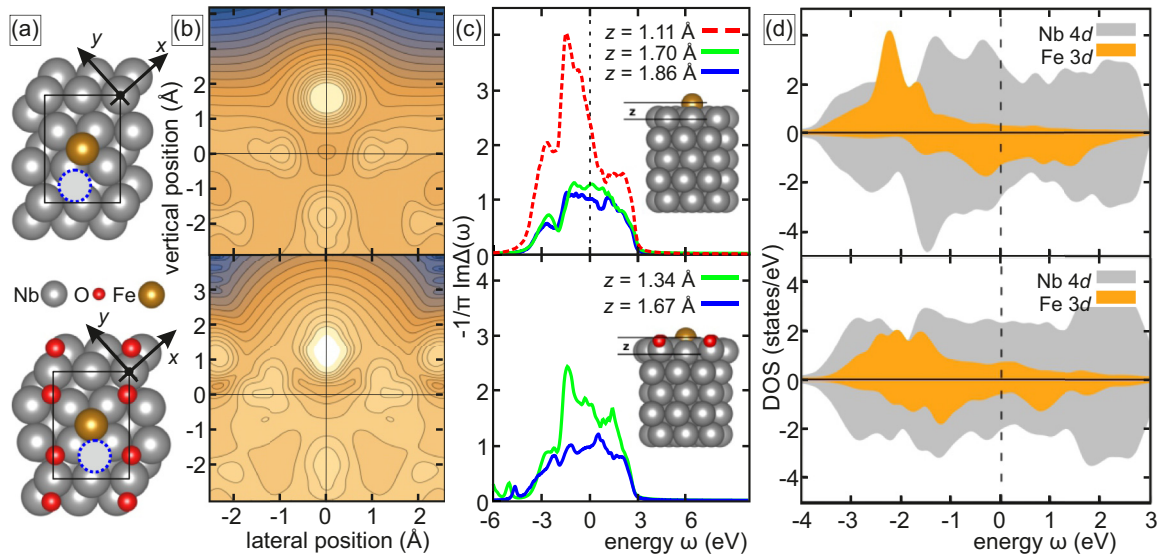


FIG. 3. Theoretical investigation of Fe atoms on clean (top) and oxygen-reconstructed (bottom) Nb(110). (a) Top view of the unit cells used for *ab initio* calculations. (b) Charge-density profiles. The higher charge density over Fe/NbO_x translates into its larger apparent height in constant-current STM images (cf. Fig. 1), despite its shorter binding distance. (c) Imaginary part of the hybridization function summed over all Fe *d* orbitals. The solid green curves refer to Fe adatoms in their equilibrium geometries shown in panel (a). The red dashed line in the top panel refers to the case of an artificially enlarged vertical distance of Fe on the clean Nb(110) surface. The solid blue lines, instead, pertain to the cases where Fe adatoms are adsorbed onto the energetically less-favorable sites highlighted by the dashed blue circles in panel (a). While on the NbO_x surface, the Fe hybridization function shows a strong dependence on the adsorption site, this is not the case for Fe adatoms on clean Nb(110). (d) DOS projected on the surface Nb (gray) and Fe (orange) *d* states. Positive and negative values correspond to majority and minority spin, respectively. The calculated LDOS of each individual orbital and the relative hybridization functions can be found in Ref. [24].

Fe atom on NbO_x than on clean Nb(110), which—in the constant-current mode of the STM—translates into a larger apparent height, as observed experimentally [cf. Fig. 1(b)].

This variation of binding distance crucially impacts the adatom-substrate coupling. Close to E_F we observe a modified form and value of the hybridization function $\Delta(\omega)$ [green solid lines in Fig. 3(c)], which describes the probability amplitude of an electron to hop from the impurity to the substrate and back. The internal orbital structure of the Fe *d* shell defines a multi-orbital Anderson impurity model. As evinced by the DFT majority- and minority-spin DOS shown in Fig. 3(d), the magnetic moment of Fe/NbO_x ($m^* = 0.9\mu_B$) amounts to less than half of the corresponding value for Fe/Nb(110) in the H_4 site ($m = 2.2\mu_B$). At the same time, the hybridization function steeply increases, Fig. 3(c), leading to an enhanced exchange interaction J for Fe/NbO_x. As will be shown, this overcompensates the reduction of the impurity moment m and effectively shifts the system into the Kondo-screened regime.

The T dependencies of the static impurity spin susceptibility $\chi_{\text{loc},\omega=0}$ and the effective screened spin $S_{\text{eff}}^{\text{scr}}$ of the Fe impurity as calculated with CT-QMC are shown in Figs. 4(a) and 4(b). For a free local moment, $\chi_{\text{loc},\omega=0}(T)$ is of Curie-Weiss type ($\propto 1/T$) and changes to a weakly T -dependent Pauli-like behavior for moments screened by conduction electrons. Although the Fe impurity will always be fully screened at $T = 0$, the way this screening takes place when lowering T can vary significantly. For the T range investigated in our calculations, Fe on clean Nb displays a Curie-Weiss susceptibility and the corresponding effective spin is still far from being fully screened. On the contrary, $\chi_{\text{loc},\omega=0}(T)$

for Fe/NbO_x exhibits a pronounced Pauli-like behavior and $S_{\text{eff}}^{\text{scr}}(T)$ is significantly reduced.

As shown in Figs. 4(a) and 4(b), our analysis of the crossover between these two physical regimes identifies the Fe-surface distance z as the driving mechanism. This is confirmed by simulating Fe on clean Nb(110) at an artificial height. Selecting a value comparable to Fe/NbO_x—see blue dashed line in Fig. 4—we observe a qualitatively similar Pauli spin response and a low $S_{\text{eff}}^{\text{scr}} \cdot T$ -dependent $S_{\text{eff}}^{\text{scr}}$ data also allow us to extract plausible hints on the respective T_K . In Fe/NbO_x, an inflection point is visible around 40 K. Below this temperature, $S_{\text{eff}}^{\text{scr}}$ decays Fermi-liquid-like, i.e., $\propto T^2$ [red-dotted line in Fig. 4(b)]. For Fe/Nb(110) no such inflection point is reached down to the lowest T , confirming that Fe/Nb(110) and Fe/NbO_x belong to different Kondo-coupling regimes.

Additionally, for Fe on clean Nb(110) at $z = 1.70 \text{ \AA}$, given the pronounced Curie-Weiss $\chi_{\text{loc},\omega=0}(T)$, we can fit the CT-QMC data to $\mu_{\text{fit}}^2/3(T + 2T_K)$, a formula valid for an intermediate temperature range [34]. The resulting susceptibility, which includes contributions from the whole *d* shell is shown as a black solid line in Fig. 4(a). Analyzing the individual, orbital-specific contributions to $\chi_{\text{loc},\omega=0}$ we see that μ_{fit} for d_{z^2} is larger than for $d_{xz,yz}$, see table inset to Fig. 4(b). We infer that the former hosts the most correlated electrons, also confirmed by the orbital-resolved values $S_{\text{eff}}^{\text{scr}}$.¹ The fit yields a

¹In this comparison we did not consider the two purely planar orbitals d_{xy} and $d_{x^2-y^2}$ since they are less relevant for tunneling into the tip.

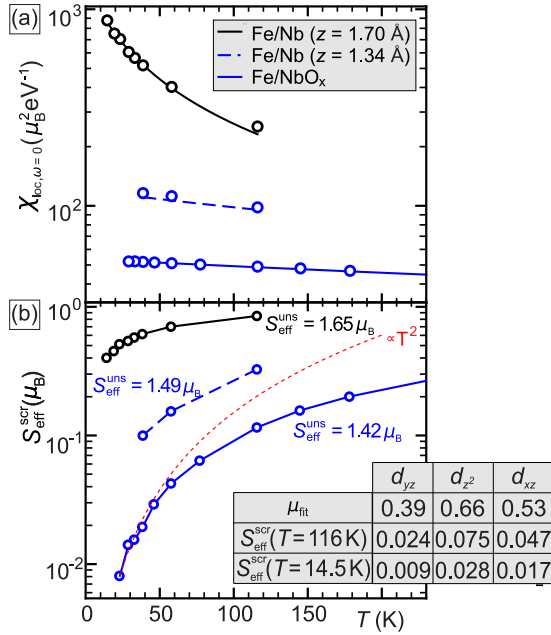


FIG. 4. (a) Temperature-dependent static local spin susceptibility and (b) effective impurity spin of Fe/Nb(110) (distances $z = 1.70$ Å and $z = 1.34$ Å) and for Fe/NbO_x ($z = 1.34$ Å). Black line is a Curie-Weiss fit with Wilson form $\mu_{\text{fit}}^2/3(T + 2T_K)$. The unscreened effective spin ($S_{\text{eff}}^{\text{uns}}$) is T independent, representing the instantaneous paramagnetic moment. When lowering T , screening via the substrate becomes increasingly effective, as shown by the $S_{\text{eff}}^{\text{scr}}(T)$ behavior obtained from the spin-spin correlation function at long (imaginary) times. Inset shows values of μ_{fit} and the screened effective spin $S_{\text{eff}}^{\text{scr}}$ (both in units of μ_B) for the three relevant orbitals of the d shell, calculated at $z = 1.70$ Å.

T_K value of the order of 10 K, i.e., four times smaller than for Fe/NbO_x.

A well-known characteristic of correlated electrons is their strong response to small changes of parameters [35–37]. Given its out-of-plane orientation, we expect that the d_{z^2} orbital is most susceptible to geometrical changes such as a variation of the adatom-substrate distance z . Therefore, the highly responsive α_{\pm} peaks probably originate from processes involving the d_{z^2} orbital. For the β_{\pm} peaks we have less stringent evidence, but most plausibly they are related to $d_{xz,yz}$ orbitals.²

Remarkably, we can draw quantitative conclusions on YSR states for the *superconducting* phase even though T_K is obtained from many-body calculations in the *normal* state [17]. To verify the claim of a direct relation between the substrate-tuned Kondo temperature and YSR states, we performed

²Let us note at this point that, while the previous orbital-resolved analysis is informative, one has to bear in mind that the diagonal contributions to $\chi_{\text{loc},\omega=0}$ and $S_{\text{eff}}^{\text{scr}}$ constitute only a small fraction of the respective full values [compare table in Fig. 4(b) with the CT-QMC curves shown in the figure]. This means that the Kondo effect in these adatoms ultimately involves five entangled (and partially filled) d orbitals and its picture as five independent Kondo channels is to be taken *cum grano salis*.

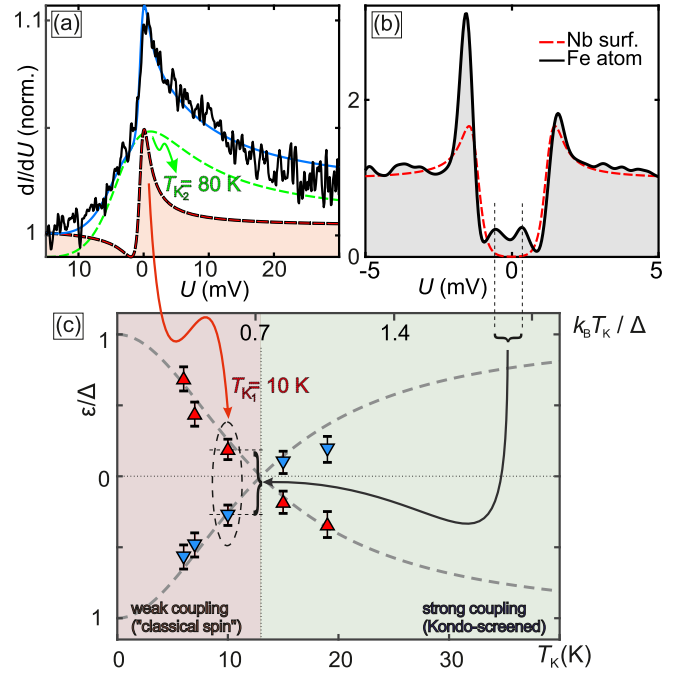


FIG. 5. Kondo resonance (a) and YSR bound states (b) measured on the same Fe atom at $T = 1.5$ K with and without external magnetic field $\mu_0 H = 0.6$ T, respectively. The Kondo resonance is fit with two Fano curves, with low $T_{K1} = 10$ K (red dashed line) and high $T_{K2} = 80$ K (green). Blue: sum of both Fano curves. (c) T_K -dependent positions of the YSR peaks measured for five individual Fe atoms. The transition occurs at $T_{K1} = 13$ K.

two-stage STS measurements on the same set of different individual Fe atoms [24]. At the first stage we investigated the Kondo effect on normal-metallic Nb(110). To suppress the superconducting state, the sample was exposed to an out-of-plane magnetic field $\mu_0 H = 0.6$ T $> \mu_0 H_{c2}$. A spectrum with the characteristic asymmetric Kondo peak is presented in Fig. 5(a). In line with the theoretical discussion above, it can be fit by two Fano curves, accounting for the interaction of the d_{z^2} and $d_{xz,yz}$ orbitals, respectively. A similar behavior was observed for Fe adatoms on Re(0001) [20]. Whereas the feature with the broader peak exhibits a rather high $T_{K2} = (75 \pm 10)$ K which is—within our error bar— independent of the particular Fe atom adsorption site, the second, more narrow feature has a much lower Kondo temperature (T_{K1}) which varies significantly between the Fe adatoms. For example, $T_{K1} = 10$ K for the particular Fe atom analyzed in Fig. 5(a).

At the second stage the magnetic field was turned off and the same Fe adatoms were investigated on superconducting Nb(110). The deconvoluted tunneling spectrum of the same Fe adatom analyzed in Fig. 5(a) is presented in Fig. 5(b). A pronounced superconducting gap and YSR in-gap peaks can be recognized. In Fig. 5(c) we summarize the data obtained from five Fe adatoms by plotting their individual YSR peak positions versus the respective lowest Kondo temperature T_{K1} . The dashed line is given by $|\varepsilon| = \Delta[(1 - a^2)/(1 + a^2)]$, i.e., the same functional form of the classical limit, but by replacing a with $k_B T_K / (0.72\Delta)$. This choice yields the best agreement with the experimental data in the explored range of T_K . At first sight it is surprising that the classical spin model

is even able to properly describe the experimental data in the strong-coupling range. However, within a more general Anderson impurity model coupled to a superconducting lead, a similar structure was found [38,39]. This more general model explicitly implies the dependence of YSR bound states on the hybridization with the substrate Γ , also embedded in the Kondo effect, including the interplay with the Andreev bound state [39]. We find a good qualitative agreement with theoretical predictions [15–17], as the transition point occurs at a critical Kondo temperature $T_{K_c} \approx 0.7\Delta$. This value is similar but slightly below the pairing parameter Δ reported for Moiré patterns of Mn-phthalocyanine molecules on Pb(111) [18,40]. Even though alternative definitions of T_K modify the position of the transition [41], the crossover always remains below the pairing parameter Δ , thereby suggesting a universal, largely template-independent quantum phase transition at a Kondo energy scale corresponding to the superconducting gap.

From a more general perspective, the results presented here may guide future efforts in creating atomic scale assemblies which hold MZMs. A necessary condition is a strong

coupling between the superconductor and the magnetic impurities, which—for Fe adatoms on Nb(110) surfaces—can only be facilitated by surface functionalization with oxygen. While this significantly increases the exchange between the superconducting substrate and the adatom, it leaves T_c essentially unaffected such that the advantages of Nb can still be fully exploited.

ACKNOWLEDGMENTS

This work was supported by the Deutsche Forschungsgemeinschaft (DFG, German Research Foundation)—Project-ID 258499086—SFB 1170 (A02/B06/C07) and through the Würzburg-Dresden Cluster of Excellence on Complexity and Topology in Quantum Matter—*ct.qmat* Project-ID 390858490 - EXC 2147. The authors acknowledge R. Žitko for useful discussions, and the Gauss Centre for Supercomputing e.V. for providing computing time on the GCS Supercomputer SuperMUC at Leibniz Supercomputing Centre.

-
- [1] S. Nadj-Perge, I. K. Drozdov, B. A. Bernevig, and A. Yazdani, Proposal for realizing Majorana fermions in chains of magnetic atoms on a superconductor, *Phys. Rev. B* **88**, 020407(R) (2013).
- [2] F. Pientka, L. I. Glazman, and F. von Oppen, Topological superconducting phase in helical Shiba chains, *Phys. Rev. B* **88**, 155420 (2013).
- [3] Bernd Braunecker and Pascal Simon, Interplay Between Classical Magnetic Moments and Superconductivity in Quantum One-Dimensional Conductors: Toward a Self-Sustained Topological Majorana Phase, *Phys. Rev. Lett.* **111**, 147202 (2013).
- [4] J. Klinovaja, P. Stano, A. Yazdani, and D. Loss, Topological Superconductivity and Majorana Fermions in RKKY Systems, *Phys. Rev. Lett.* **111**, 186805 (2013).
- [5] M. M. Vazifeh and M. Franz, Self-Organized Topological State with Majorana Fermions, *Phys. Rev. Lett.* **111**, 206802 (2013).
- [6] Y. Kim, M. Cheng, B. Bauer, R. M. Lutchyn, and S. Das Sarma, Helical order in one-dimensional magnetic atom chains and possible emergence of Majorana bound states, *Phys. Rev. B* **90**, 060401(R) (2014).
- [7] S. Nadj-Perge, I. K. Drozdov, J. Li, H. Chen, S. Jeon, J. Seo, A. H. MacDonald, B. A. Bernevig, and A. Yazdani, Observation of Majorana fermions in ferromagnetic atomic chains on a superconductor, *Science* **346**, 602 (2014).
- [8] H. Kim, A. Palacio-Morales, T. Posske, L. Rózsa, K. Palotás, L. Szunyogh, M. Thorwart, and R. Wiesendanger, Toward tailoring Majorana bound states in artificially constructed magnetic atom chains on elemental superconductors, *Sci. Adv.* **4**, eaar5251 (2018).
- [9] A. Kamlapure, L. Cornils, J. Wiebe, and R. Wiesendanger, Engineering the spin couplings in atomically crafted spin chains on an elemental superconductor, *Nat. Commun.* **9**, 3253 (2018).
- [10] L. Yu, Bound state in superconductors with magnetic impurities, *Acta Phys. Sin.* **21**, 75 (1965).
- [11] H. Shiba, Classical spins in superconductors, *Prog. Theor. Phys.* **40**, 435 (1968).
- [12] A. I. Rusinov, Superconductivity near a paramagnetic impurity, *ZhETF Pis. Red.* **2**, 146 (1969) [*JETP Lett.* **9**, 85 (1969)].
- [13] J. Kondo, Resistance minimum in dilute magnetic alloys, *Prog. Theor. Phys.* **32**, 37 (1964).
- [14] T. Matsuura, S. Ichinose, and Y. Nagaoka, Theory of Kondo effect in superconductors. I: Transition temperature and upper critical field, *Prog. Theor. Phys.* **57**, 713 (1977).
- [15] K. Satori, H. Shiba, O. Sakai, and Y. Shimizu, Numerical renormalization group study of magnetic impurities in superconductors, *J. Phys. Soc. Jpn.* **61**, 3239 (1992).
- [16] O. Sakai, Y. Shimizu, H. Shiba, and K. Satori, Numerical renormalization group study of magnetic impurities in superconductors. II. Dynamical excitation spectra and spatial variation of the order parameter, *J. Phys. Soc. Jpn.* **62**, 3181 (1993).
- [17] R. Žitko, O. Bodensiek, and T. Pruschke, Effects of magnetic anisotropy on the subgap excitations induced by quantum impurities in a superconducting host, *Phys. Rev. B* **83**, 054512 (2011).
- [18] K. J. Franke, G. Schulze, and J. I. Pascual, Competition of superconducting phenomena and Kondo screening at the nanoscale, *Science* **332**, 940 (2011).
- [19] N. Hatter, B. W. Heinrich, D. Rolf, and K. J. Franke, Scaling of Yu-Shiba-Rusinov energies in the weak-coupling Kondo regime, *Nat. Commun.* **8**, 2016 (2017).
- [20] L. Schneider, M. Steinbrecher, L. Rózsa, J. Bouaziz, K. Palotás, M. dos Santos Dias, S. Lounis, J. Wiebe, and R. Wiesendanger, Magnetism and in-gap states of 3d transition metal atoms on superconducting Re, *npj Quantum Mater.* **4**, 42 (2019).
- [21] S. Kezilebieke, R. Žitko, M. Dvorak, T. Ojanen, and P. Liljeroth, Observation of coexistence of Yu-Shiba-Rusinov states and spin-flip excitations, *Nano Lett.* **19**, 4614 (2019).
- [22] H. Huang, R. Drost, J. Senkpiel, C. Padurariu, B. Kubala, A. L. Yeyati, J. C. Cuevas, J. Ankerhold, K. Kern, and C. R. Ast, Magnetic impurities on superconducting surfaces: Phase transi-

- tions and the role of impurity-substrate hybridization, *Commun. Phys.* **3**, 199 (2020).
- [23] A. B. Odobesko, S. Haldar, S. Wilfert, J. Hagen, J. Jung, N. Schmidt, P. Sessi, M. Vogt, S. Heinze, and M. Bode, Preparation and electronic properties of clean superconducting Nb(110) surfaces, *Phys. Rev. B* **99**, 115437 (2019).
- [24] See supplemental material at <http://link.aps.org/supplemental/10.1103/PhysRevB.102.174504> for detailed information regarding deconvolution methods, details of theoretical methods, the calculated Fe atom magnetic moments, orbital-resolved LDOS of Fe on Nb(110), and additional data for Kondo temperature determination, which includes Refs. [42–47].
- [25] G. Kresse and J. Furthmüller, Efficient iterative schemes for *ab initio* total-energy calculations using a plane-wave basis set, *Phys. Rev. B* **54**, 11169 (1996).
- [26] M. Wallerberger, A. Hausoel, P. Gunacker, A. Kowalski, N. Parragh, F. Goth, K. Held, and G. Sangiovanni, w2dynamics: Local one- and two-particle quantities from dynamical mean field theory, *Comput. Phys. Commun.* **235**, 388 (2019).
- [27] A. Hausoel, M. Karolak, E. Sasioglu, A. Lichtenstein, K. Held, A. Katanin, A. Toschi, and G. Sangiovanni, Local magnetic moments in iron and nickel at ambient and Earth’s core conditions, *Nat. Commun.* **8**, 16062 (2017).
- [28] M. I. Salkola, A. V. Balatsky, and J. R. Schrieffer, Spectral properties of quasiparticle excitations induced by magnetic moments in superconductors, *Phys. Rev. B* **55**, 12648 (1997).
- [29] M. E. Flatté and J. M. Byers, Local electronic structure of defects in superconductors, *Phys. Rev. B* **56**, 11213 (1997).
- [30] L. Cornils, A. Kamlapure, L. Zhou, S. Pradhan, A. A. Khajetoorians, J. Fransson, J. Wiebe, and R. Wiesendanger, Spin-Resolved Spectroscopy of the Yu-Shiba-Rusinov States of Individual Atoms, *Phys. Rev. Lett.* **119**, 197002 (2017).
- [31] M. Getzlaff, J. Bansmann, and G. Schönhense, Oxygen on Fe(110): Magnetic properties of the adsorbate system, *J. Magn. Mater.* **192**, 458 (1999).
- [32] F. Passek and M. Donath, Magnetic Surface State Becomes Nonmagnetic by Oxygen Adsorption, *Phys. Rev. Lett.* **71**, 2122 (1993).
- [33] D. N. McIlroy, C. Waldfried, D. Li, J. Pearson, S. D. Bader, D.-J. Huang, P. D. Johnson, R. F. Sabiryanov, S. S. Jaswal, and P. A. Dowben, Oxygen Induced Suppression of the Surface Magnetization of Gd(0001), *Phys. Rev. Lett.* **76**, 2802 (1996).
- [34] K. G. Wilson, The renormalization group: Critical phenomena and the Kondo problem, *Rev. Mod. Phys.* **47**, 773 (1975).
- [35] M-Imada, A. Fujimori, and Y. Tokura, Metal-insulator transitions, *Rev. Mod. Phys.* **70**, 1039 (1998).
- [36] P. Limelette, Universality and critical behavior at the Mott transition, *Science* **302**, 89 (2003).
- [37] J. Kügel, M. Karolak, A. Krönlein, D. Serrate, M. Bode, and G. Sangiovanni, Reversible magnetic switching of high-spin molecules on a giant Rashba surface, *npj Quantum Mater.* **3**, 53 (2018).
- [38] Rok Žitko, Jong Soo Lim, Rosa López, and Ramón Aguado, Shiba states and zero-bias anomalies in the hybrid normal-superconductor Anderson model, *Phys. Rev. B* **91**, 045441 (2015).
- [39] A. Villas, R. L. Klees, H. Huang, C. R. Ast, G. Rastelli, W. Belzig, and J. C. Cuevas, Interplay between Yu-Shiba-Rusinov states and multiple Andreev reflections, *Phys. Rev. B* **101**, 235445 (2020).
- [40] J. Bauer, J. I. Pascual, and K. J. Franke, Microscopic resolution of the interplay of Kondo screening and superconducting pairing: Mn-phthalocyanine molecules adsorbed on superconducting Pb(111), *Phys. Rev. B* **87**, 075125 (2013).
- [41] A. C. Hewson, *The Kondo Problem to Heavy Fermions* (Cambridge University Press, Cambridge, 1993).
- [42] D.-J. Choi, C. Rubio-Verdú, J. de Bruijckere, M. M. Ugeda, N. Lorente, and J. I. Pascual, Mapping the orbital structure of impurity bound states in a superconductor, *Nat. Commun.* **8**, 15175 (2017).
- [43] S. Twomey, On the numerical solution of Fredholm integral equations of the first kind by the inversion of the linear system produced by quadrature, *J. Assoc. Comput. Mach.* **10**, 97 (1963).
- [44] M. Ternes, A. J. Heinrich, and W.-D. Schneider, Spectroscopic manifestations of the kondo effect on single adatoms, *J. Phys.: Condens. Matter* **21**, 053001 (2008).
- [45] P. E. Blöchl, Projector augmented-wave method, *Phys. Rev. B* **50**, 17953 (1994).
- [46] G. Kresse and D. Joubert, From ultrasoft pseudopotentials to the projector augmented-wave method, *Phys. Rev. B* **59**, 1758 (1999).
- [47] R. C. Dynes, V. Narayanamurti, and J. P. Garno, Direct Measurement of Quasiparticle-Lifetime Broadening in a Strong-Coupled Superconductor, *Phys. Rev. Lett.* **41**, 1509 (1978).